Dynamically Reversible Iron Oxide Nanoparticle Assemblies for Targeted Amplification of T1-Weighted Magnetic Resonance Imaging of Tumors

Fangyuan Li,[†,‡,O] Zeyu Liang,[†,O] Jianan Liu,[∥,⊥,O] Jihong Sun,[§] Xi Hu,[†] Meng Zhao,[†] Jiaxin Liu,[§] Ruiliang Bai,[∇] Dokyoon Kim,[∥,⊥] Xiaolian Sun,[#] Taeghwan Hyeon,[∥,⊥] and Daishun Ling*,[†,▲,‡]

[†]Institute of Pharmaceutics and [▲]Hangzhou Institute of Innovative Medicine, College of Pharmaceutical Sciences, Zhejiang University, Hangzhou 310058, China

[‡]MOE Key Laboratory of Biomedical Engineering, College of Biomedical Engineering and Instrument Science, Zhejiang University, Hangzhou 310058, China

[§]Department of Radiology, Sir Run Run Shaw Hospital, School of Medicine, Zhejiang University, Hangzhou 310020, China

[∥]Center for Nanoparticle Research, Institute for Basic Science (IBS), Seoul 08826, Republic of Korea

[⊥]School of Chemical and Biological Engineering, Seoul National University, Seoul 08826, Republic of Korea

[#]Department of Pharmaceutical Analysis, China Pharmaceutical University, Nanjing 210009, China

[∇]Interdisciplinary Institute of Neuroscience and Technology, Qiushi Academy for Advanced Studies, College of Biomedical Engineering and Instrument Science, Zhejiang University, Hangzhou, China, 310029

S Supporting Information

ABSTRACT: Smart magnetic resonance (MR) contrast agents, by which MR contrast can be selectively enhanced under acidic tumor microenvironment, are anticipated to significantly improve the diagnostic accuracy. Here, we report pH-sensitive iron oxide nanoparticle assemblies (IONAs) that are cross-linked by small-molecular aldehyde derivative ligands. The dynamic formation and cleavage of hydrazone linkages in neutral and acidic environments, respectively, allow the reversible response of the nanoassemblies to pH variations. At neutral pH, IONAs are structurally robust due to the cross-linking by the strong hydrazone bonds. In acidic tumor microenvironment, the hydrazone bonds are cleaved so that the IONAs are quickly disassembled into a large number of hydrophilic extremely small-sized iron oxide nanoparticles (ESIONs). As a result, significantly enhanced T1MR contrast is achieved, as confirmed by the measurement of $r1$ values at different pH conditions. Such acidity-targeting MR signal amplification by the pH-sensitive IONAs was further validated in vivo, demonstrating a novel T1 magnetic resonance imaging (MRI) strategy for highly sensitive imaging of acidic tumors.

KEYWORDS: Dynamic assembly, iron oxide nanoparticle, pH-sensitive, T1MR imaging, tumor diagnosis
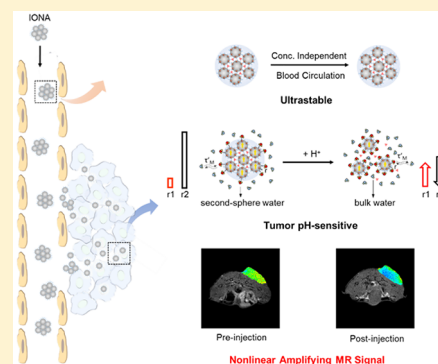
MRI, as an integral noninvasive imaging tool in clinical diagnosis, can identify anatomical details of various diseases by precise soft tissue contrast.[1−3] Its sensitivity has been largely improved with the development of chemically engineered high-performance imaging agents, such as gadolinium (Gd) and iron oxide nanoparticle-based MR contrast agents.[4−7] For the nanoparticle-based contrast agents, their controlled assembly can provide a unique approach to manipulate the collective magnetic properties of the nanoparticles that directly influence their MR contrast effects.[8−10] For example, iron oxide nanoparticle assemblies assisted by bioresponsive surface ligands exhibit stimuli-responsive image contrasting behavior, which is useful to enhance the imaging quality and specificity of MRI.[11−15]

However, most currently available stimuli-sensitive iron oxide nanoparticle assemblies are T2MR contrast agents, whose clinical translations are hampered by intrinsic disadvantages such as blooming effects and confusion with hypointense areas.[16,17] In contrast, T1MR contrast agents are preferred for accurate high-resolution imaging in clinical settings.[18,19] Particularly, some pH-responsive Gd-based chelates or nanoparticle assemblies can easily increase their longitudinal relaxivity ($r1$) under tumor microenvironment and therefore specifically lighten the tumor regions.[20−22] However, even a very small amount of free Gd ions leached from these contrast agents has been demonstrated to be very toxic.[16,23] In 2017, the US Food and Drug Administration
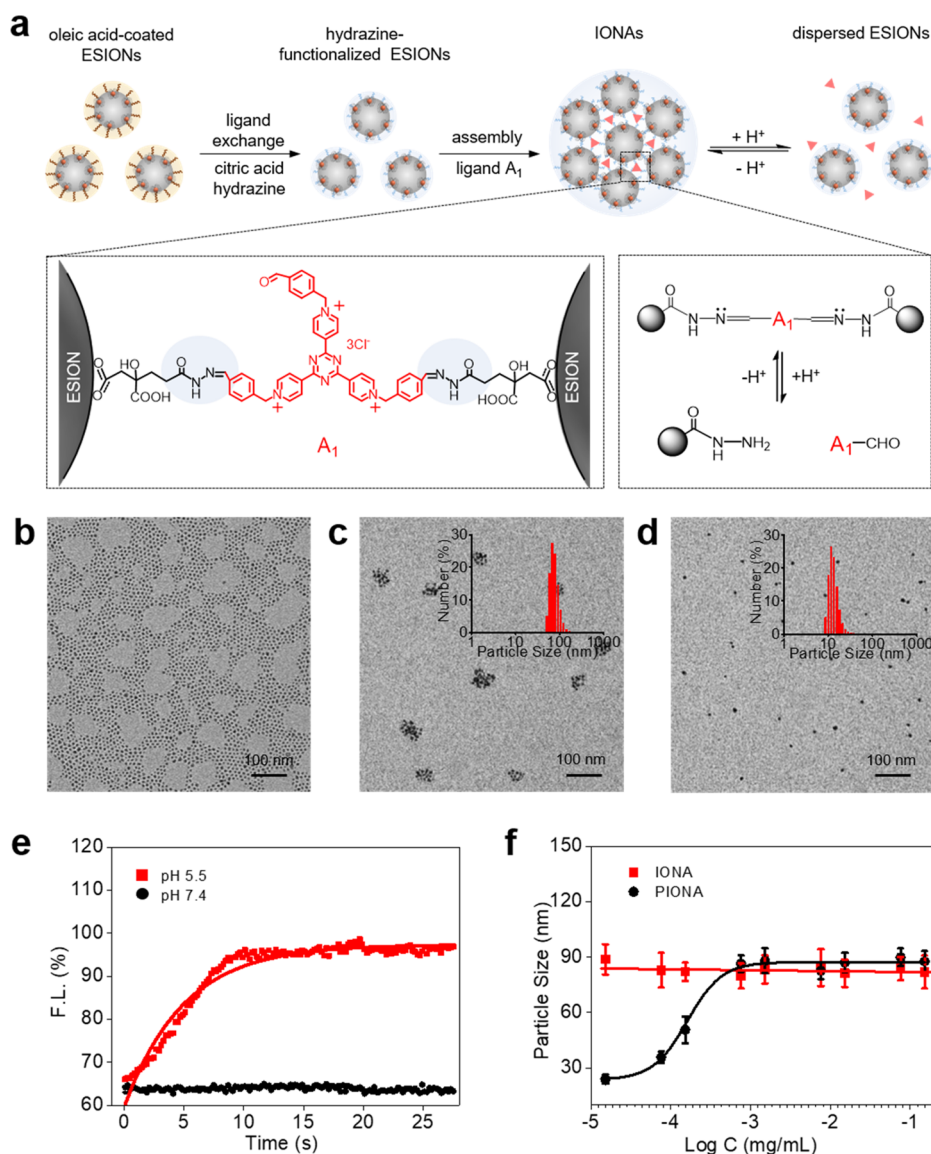
Figure 1. Design, synthesis, and characterization of IONAs. (a) Schematic illustration of IONA formation and its pH-triggered disassembly. Hydrazine-functionalized ESIONs are chemically linked by ligand A_1 to form IONAs, which disassemble into dispersed ESIONs in acidic medium. (b−d) TEM images of ESIONs in chloroform, IONAs in water at pH 7.4 and 5.5, respectively. Inset: hydrodynamic size of IONAs at pH 7.4 and 5.5, respectively. (e) Kinetic study of IONA disassembly at pH 5.5. (f) Size variations of IONAs and PIONAs under different Fe concentrations from 1.5×10^{-5} to 0.15 mg/mL.

(FDA) warned that the employment of Gd-based contrast agents will inevitably induce Gd deposition in the brain or bone. While the assemblies of biocompatible extremely small-sized iron oxide nanoparticles (ESIONs) with pH-sensitive polymeric ligands have emerged as a potential alternative for enhancing T1MRI,[24,25] their efficiency is often diminished due to the presence of hydrophobic ligands (e.g., oleic acid, oleylamine, trialkylphosphine, and so forth) on their surface.[26] After the disassociation of the assemblies in acidic micro-environment, these hydrophobic coatings on individual ESIONs can greatly suppress their water accessibility, resulting in minimally enhanced T1MR signal. Such relatively small changes in $r1$ and $r2/r1$ values make the ESION assembly-based MR contrast agents unsuitable for pH-sensitive T1MR imaging.[27−29] Moreover, such polymer-based pH-sensitive assembly agents can convey false information in vivo as the disassembly process is initiated not only by the acidic

microenvironment but also under diluted conditions where the polymer concentration is below its critical aggregation concentration (CAC).[30−33]

Herein, we report in vivo stable iron oxide nanoparticle assemblies (IONAs) based on hydrazone linkage (−C=N−N−) for targeted enhancement of T1-weighted MRI of acidic tumors (Figure 1a). ESIONs prepared by a previously reported method (Figure 1b) were first transferred into an aqueous medium, resulting in a hydrodynamic diameter of ~7 nm (Figure S1), via ligand exchange with citric acid.[16,34] The initial oleic acid ligands of ESIONs were completely substituted with hydrophilic citric acid to enable their full access to water molecules for favorable T1 relaxation. Hydrazine was then introduced to generate hydrazide groups on the ESION surface via condensation reactions. The hydrazine-functionalized ESIONs were well-dispersed in water with a hydrodynamic diameter of ~9 nm (Figure S2). To form IONAs, the aldehyde
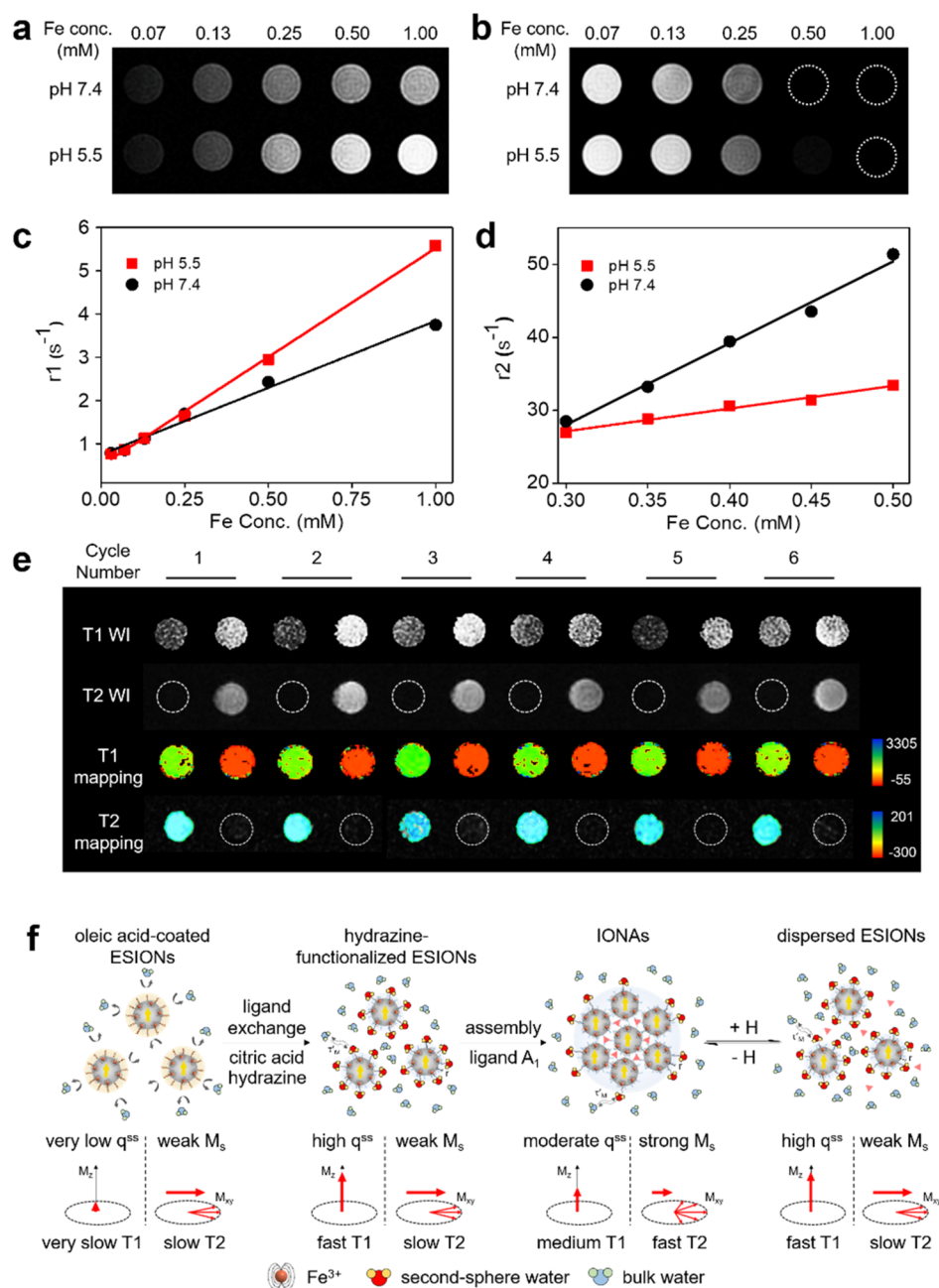
Figure 2. pH-sensitive MRI properties of IONAs. (a,b) T1- and T2-weighted images (WI) of IONAs at pH 7.4 and 5.5. (c,d) $r1$ and $r2$ values of IONAs at pH 7.4 and 5.5. (e) Six complete assembly/disassembly cycles between pH 7.4 and 5.5 as measured by MRI. (f) Schematic illustration of pH-triggered nonlinearly amplified MR signal using IONAs. The q^{SS} and magnetic field inhomogeneity are the main factors affecting the T1 and T2 relaxations of water protons, respectively. M_{xy} and M_z represent the net nuclei spins on the transverse (M_{xy}) and longitudinal (M_z) planes, respectively.

derivative ligand A_1 was synthesized (Figure S3) and used as a linker to connect the hydrazine-functionalized ESIONs through hydrazone bonds, which are highly stable under neutral aqueous conditions but can be cleaved under acidic conditions.[35,36] Transmission electron microscopy (TEM) images and dynamic light scattering (DLS) measurements revealed that IONAs have a quasi-spherical shape of ~60 nm in diameter and are well-dispersed in aqueous solution with a hydrodynamic diameter of ~80 nm (Figure 1c). X-ray diffraction (XRD) patterns revealed the maghemite (γ-Fe$_2$O$_3$; JCPDS no. 39-1346) crystal structure of IONAs (Figure S4), indicating no change in crystal structure compared with

ESIONs. The acylhydrazone linker in IONAs was verified by Fourier transform infrared spectroscopy (FT-IR) (Figure S5). By adjusting the mass ratio between the ligands and the ESIONs, we found that the assembly can be formed only when the ratio range of A_1 ligands to hydrazine-functionalized ESIONs is from 1:10 to 6:1 (Figure S6). Thus, it could be speculated that a small amount of A_1 ligands is insufficient to initiate the formation of acylhydrazone linker, while excess A_1 ligands hinder their assembly.[37] Specifically, when the ratio of A_1 ligands to hydrazine-functionalized ESIONs is less than 1:10, there are not enough ligands to cross-link ESIONs into the assembly structure; However, with increasing the ratio to

1:10−6:1, sufficient ligands become available to cross-link a partial number of ESIONs for forming the assembly structure. In this case, the chemical bond formation and the electrostatic repulsion between the ESIONs will operate in mutually opposite ways to restrict the final size of the IONAs; Once the ratio is higher than 6:1, the number of ligands is enough to cover all the ESIONs individually without resulting in the partial cross-linking between the ESIONs. Because of the positive charge of the A_1 ligand, individually coated ESIONs remain dispersed in solution rather than forming the nanoassemblies.

The pH-dependent structural transformation was characterized by TEM. At neutral pH, IONAs maintain the assembly structure (Figure 1c), while at acidic pH, the hydrazone bonds in IONAs begin to "loosen" due to the ionization of the imine moieties. As the pH further decreases, hydrazine functionalized ESIONs start repelling each other, eventually resulting in complete disassembly (Figure 1d). Importantly, oleic acid chains previously present on the surface of ESIONs were completely substituted with hydrophilic small-molecular ligands to allow the full access of the ESIONs to the environmental water molecules once the disassembly of IONAs occurs. Both size and ζ-potential measurements confirmed the pH-dependent structural sensitivity of IONAs (Figure S7). In addition, such assembly/disassembly behavior triggered by pH variation is reversible at least for six cycles, demonstrating the reliable pH-sensitive property of cross-linked IONAs (Figure S8). Kinetic analysis of the IONA disassembly was performed after labeling them with rhodamine isothiocyanate (RITC) as an indicator. According to the fitting curve of fluorescence data, it takes only ∼13.2 s for IONAs to completely disassemble into dispersed ESIONs at pH 5.5, where the half disassembly time of IONAs was calculated to be ∼4.5 s (Figure 1e and Figure S9). This fast disassembly response of IONAs allows the immediate MRI detection of the tumor in acidic environments. In contrast, when pH-insensitive cross-linked iron oxide nanoparticle assemblies (Ins−IONAs) with a similar size as IONAs were tested as a control, their size remained almost unchanged regardless of the pH variation (see the synthesis, detailed structure, and characterization in Figure S10).

Moreover, the pH-sensitive IONAs were highly stable in water, fetal bovine serum (FBS), and Dulbecco's modified eagle medium (DMEM) (Figure S11) at neutral pH. The leached amount of Fe ions from 0.25 mg IONAs was ∼38 ng even after 1 week (Figure S12), which is sufficiently low enough to avoid the potential in vivo toxicity inducible by Fe ions.[38] In addition, we did not observe any obvious change in the hydrodynamic size of the released ESIONs from IONAs at pH 5.5 (Figure S13). Thanks to the strong hydrazone bonds between each ESION in IONAs, the structural stability of the IONAs was proven to be independent of the Fe concentration, which is critical for their in vivo physiological stability as they are highly diluted in the blood flow (Figure 1f and Figure S14). Such property is essentially different from the micelle-like pH-sensitive polymer-assisted iron oxide nanoparticle assemblies (PIONAs, see the synthesis, detailed structure, and characterization in Figures S15 and S16), which can be easily dissociated in a diluted solution when the Fe concentration is less than 10^{-3} mg/mL (Figure 1f).

The relaxometric properties of nanoassemblies were investigated using a 3T MR scanner. IONAs showed an r1 value of 3.2 mM^{-1}·s^{-1} and a transverse relaxivity (r2) value of 108.0 mM^{-1}·s^{-1} at pH 7.4. As pH decreased to 5.5, r1 increased to 5.1 mM^{-1}·s^{-1} and r2 decreased to 21.3 mM^{-1}·s^{-1} (Figure 2a−d). Regardless of the small amount of Fe ion release from the dispersed ESIONs after the disassembly of IONAs at pH 5.5, the relevant T1 intensity showed no obvious change at least for 5 days (Figure S17). This pH-sensitive MR signal change of the IONAs was fully reversible under successive pH variations between pH 7.4 and 5.5 (Figure 2e and Figure S18). In control experiments, the relaxivities of Ins−IONAs were not sensitive to the given pH variations (Figure S19). In general, contrast agents with r2/r1 smaller than 5 are considered as T1 agents, while the others are mainly T2 agents.[29] The r2/r1 values of IONAs at pH 7.4 and 5.5 were estimated to be ∼34.2 and ∼4.1, respectively, indicating that the dispersed ESIONs can be regarded as a T1 contrast agent. To demonstrate the advantages of such small-molecular ligand-based nanoassemblies over the conventional polymer-based PIONAs, we also investigated the T1MR performance of assembled and disassembled PIONAs. As shown in Figure S20, PIONAs are not appropriate as a T1 agent, because the disassembly of PIONAs showed only a slight enhancement from 2.1 to 2.5 mM^{-1}·s^{-1}, and the r2/r1 value was as high as ∼11.3.

We next investigated the mechanism involved with the significant difference in acid-triggered T1MR enhancement between IONAs and PIONAs. In principle, T1-weighted MR contrast agents introduce a brighter signal by shortening the longitudinal relaxation time (T1) of protons in water molecules. According to the Solomon−Bloembergen−Morgan (SBM) theory, second-sphere relaxivity ($r1^{SS}$), which concerns the water protons not directly bonded to the paramagnetic ions at the particle surface, makes the most important contribution to the r1 value of these T1 contrast agents.[29,39,40] r1 can be further given as[29,39,41]

$$r_1 = \frac{\frac{q^{ss}}{[H_2O]}}{T'_{1M} + \tau'_M} \quad (1)$$

$$\frac{1}{T'_{1M}} = \frac{2}{15}\left(\frac{\mu_0}{4\pi}\right)\left(\frac{\gamma_H^2 g_e^2 \mu_B^2 S(S+1)}{r^6}\right)\left[\frac{3\tau_c}{1 + w_H^2\tau_c^2}\right] \quad (2)$$

$$\frac{1}{\tau_c} = \frac{1}{\tau'_M} + \frac{1}{\tau_R} + \frac{1}{T_{1e}} \quad (3)$$

where q^{SS} is the hydration number in the second-sphere; T'_{1M} and τ'_M are the T1 relaxation time and residency time of water molecules in the second-sphere, respectively; r is the distance between the surface metal center and water molecules; τ_c is the correlation time, which describes the fluctuating magnetic dipole; τ_R is the rotational correlation time of the contrast agent; T_{1e} characterizes the electronic T1 relaxation process; ω_H, μ_0, γ_H, g_e, and S are the constants that represent the Larmor frequency of the proton (rad/s), the Bohr magneton constant, gyromagnetic ratio of the proton, electronic g-factor, and the spin quantum number of the metal species, respectively. As indicated by the above equations, q^{SS}, r, τ'_M, and τ_R are the four variable factors influencing the second-sphere contribution (detailed theoretical deduction is provided in SI). Among them, two influential factors (r and τ'_M) remain nearly unchanged for both IONAs and their disassemblies, as they have similar coating thickness and chemical environments. As for τ_R, it seems that the introduced abundant secondary
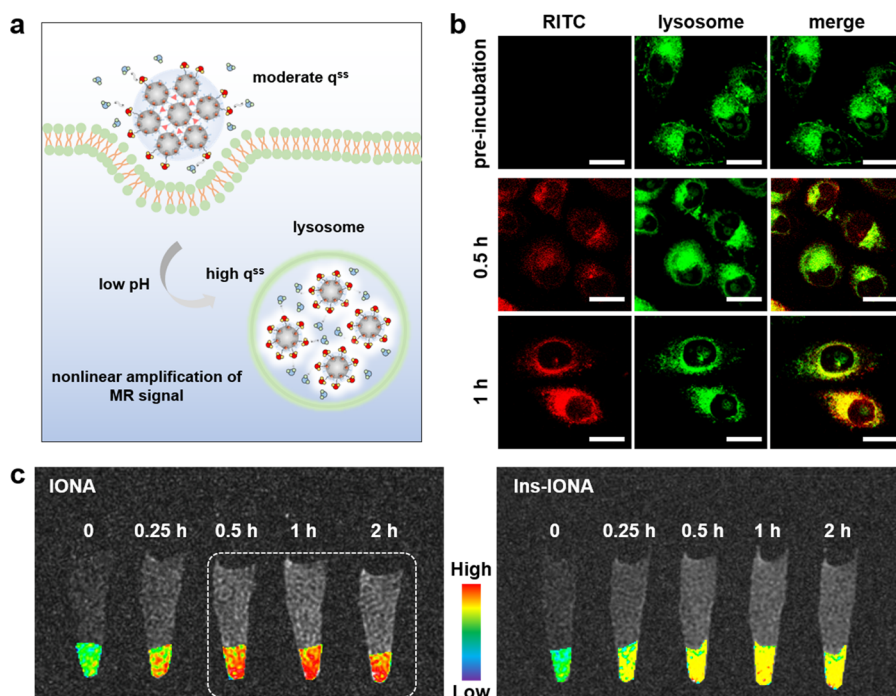
Figure 3. In vitro amplification of MR signal in tumor cells by IONAs. (a) Schematic illustration of MR imaging using IONAs. The disassembly of IONAs is triggered by acidic environment of cancer cells to result in nonlinear amplification of the MR signal. (b) CLSM images of A549 cells before and after incubation with IONAs for different time durations (0.5 and 1 h). The endo/lysosomes (green) were stained by Lysotracker Green while IONAs (red) were stained by RITC (scale bar = 20 μm). (c) T1-weighted MR images of A549 cancer cell pellets (4×10^6 cells) incubated with IONAs (left) or Ins−IONAs (right) at different incubation time points (0, 0.25, 0.5, 1, and 2 h).

bonds (i.e., hydrogen bonds) among the ESIONs increased the structural rigidity, which may potentially enhance the $r1$ relaxivity by slowing down the τ_R.[29,41] However, τ_R value is typically very high for nanoparticle-based contrast agents, which makes the $r1$ relaxivity of nanoparticle-based contrast agents little influenced by the variation of τ_R. Thus, q^{SS} becomes the deciding factor of the $r1$ value, which is related with the water accessibility to the ESION surface.[29]

As for iron oxide nanoparticles, their T1 contrast effects mainly arise from five unpaired electrons of ferric (Fe^{3+}) ions in the magnetically disordered spin layers, which effectively accelerate the protons of water molecules in the T1 relaxation process.[16,42] In neutral environment, both IONAs and PIONAs, considered as a large magnetic sphere of several ESIONs tightly packed,[43] will prevent the bulk water molecules from accessing second-sphere of inner ESIONs. These nanoassemblies can only exhibit moderate q^{SS} and medium T1 relaxation of water protons, resulting in relatively low $r1$ values. In addition, each adjacent ESION in IONAs generates local field that induces strong magnetic field inhomogeneity. Such a phenomenon causes relatively strong saturation magnetization (M_s) of IONAs and accelerates the dephasing of water protons, making them exhibit fast T2 relaxation.[10] In acidic microenvironment, the hydrophobic ESIONs dissociated from PIONAs can hardly approach any bulk water molecules due to the existence of the oleic acid on the nanoparticles surface, resulting in very small q^{SS} and therefore slow T1 relaxation of water protons. In sharp contrast, for entirely hydrophilic ESIONs obtained by using small-molecular ligands of citric acid and hydrazine to substitute the oleic acid, abundant bulk water molecules can easily access the particle second-sphere and are effectively perturbed by Fe^{3+} ions on the nanoparticle surface, endowing

these nanoparticles with large q^{SS} and fast T1 relaxation of water protons. Meanwhile, the dispersed ESIONs greatly reduce the magnetic field inhomogeneity, which results in weak M_s and makes the protons of water molecules have relatively slow T2 relaxation. As a result, such an acid-triggered nonlinear amplification in the MR signal of IONAs mainly originates from both the increased q^{SS} and the reduced magnetic field inhomogeneity of the dispersed ESIONs, which contribute to the increase of $r1$ value and the decrease of $r2$ value, respectively (Figure 2f). These theoretical explanations may guide the future design and synthesis of various responsive nanoparticle MR agents with high performances.

We further compared the surface properties of IONAs and PIONAs to support the mechanic explanation of their significant differences in acid-responsive r1 manifestation. As confirmed by FT-IR results (Figure S21), oleic acid segments existed in the disassembled PIONAs but not in the disassembled IONAs. Moreover, compared with the disassembled IONAs, the disassembled PIONAs have higher organic content (51.9 versus 28.5%) as revealed by the thermalgravimetric analysis (TGA) (Figure S22). High-resolution transmission electron microscopy (HRTEM) indicated that no obvious organic layer was coated on the ESIONs disassembled from IONAs, while numerous polymeric segments were wrapped on the nanoparticle cores in the disassembled PIONA sample (Figure S23). DLS results (Figure S24) revealed that the hydrodynamic size of dispersed ESION disassembled from IONAs is ∼17 nm, which is smaller than that from the disassembled PIONAs (∼30 nm) in water. Thus, compared with the ESIONs from IONAs, we hypothesize that the oleic acid-coated ESIONs released from PIONAs would partly capture the hydrophobic segments of residual amphipathic polymeric chains, leading to the less
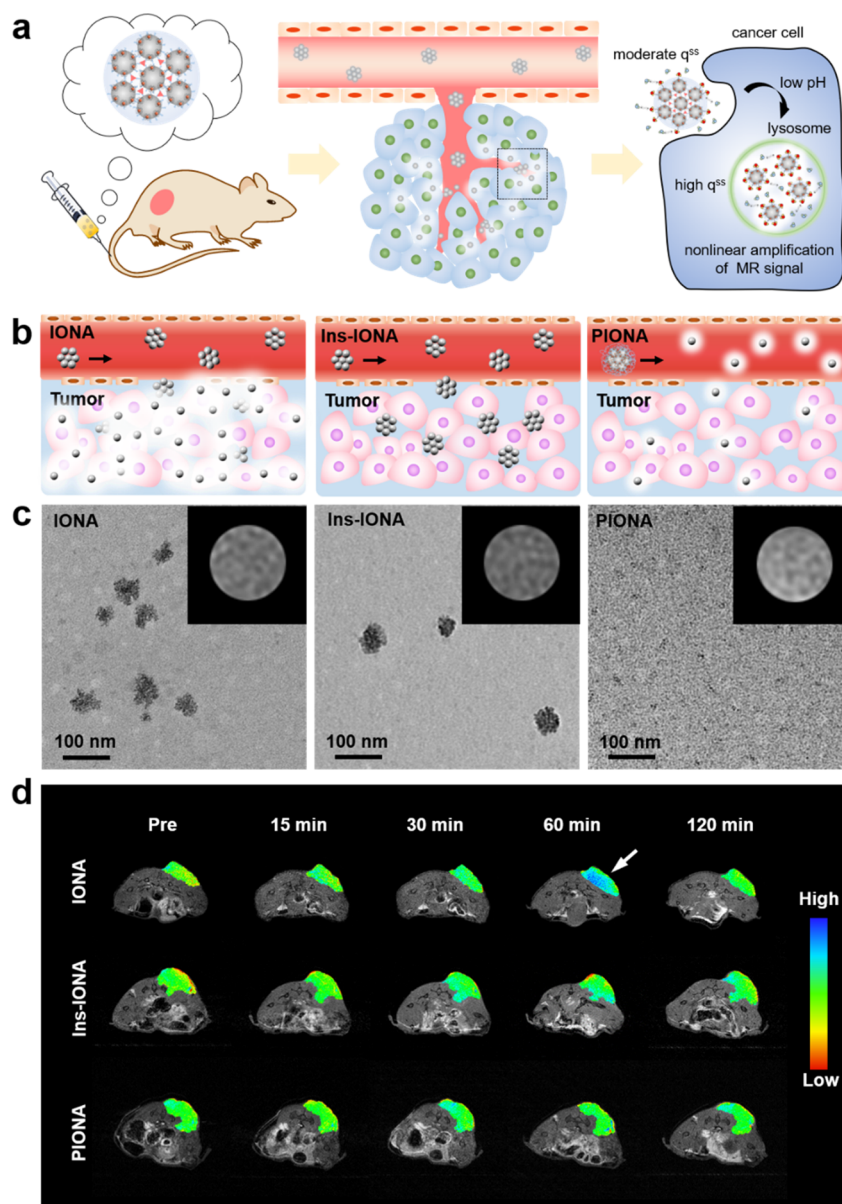
Figure 4. In vivo targeted amplification of T1-weighted MRI of tumors by IONAs. (a) Schematic illustration of MR imaging using IONAs. After i.v. injection, cross-linked IONAs accumulate in the tumor and are further pH-triggered for amplified tumor MR imaging. (b) Schematic illustration of the structural changes of IONAs, Ins–IONAs, and PIONAs in blood flow. The IONAs and Ins–IONAs are stable in blood circulation. After accumulation in tumor, IONAs further disassemble into dispersed ESIONs for nonlinear amplification of MR imaging, while Ins–IONAs remain in the quenched T1MR state. PIONAs gradually dissociate during the blood circulation even before their accumulation in tumor. (c) TEM and T1-weighted MR (inset) images of IONAs, Ins–IONAs, and PIONAs in blood. (d) T1-weighted MR images of tumor-bearing mice before and after i.v. injection of IONAs, Ins–IONAs, and PIONAs.

hydrophilic nanoparticles with greatly reduced accessibility to water molecules. Consequently, limited increase in q^{SS} and relatively slow T1 relaxation of water protons are observed.[28,44,45] The lower $r2$ value of the disassembled PIONAs was also caused by the reduction of magnetic field inhomogeneity; therefore, the T1MR contrasting effect of the PIONAs was mainly due to the decrease of $r2/r1$, rather than the inherent enhancement of $r1$ after dissociation (Figure S25).

On the basis of the above results, we further investigated the performance of IONAs in the acid-triggered enhancement of cellular T1MR signals (Figure 3a). The disassembled components of IONAs, ligand A_1, and hydrazine-functionalized ESIONs, as well as the assembled IONAs were

confirmed to be highly biocompatible to the cultured cells (Figure S26), which corroborates well with the previously reported iron-based contrast agents.[46] According to the previous studies, the derivatives of ligand A_1 could be used as safe vectors for gene delivery.[47−50] IONAs were further labeled with RITC to investigate the cellular internalization by confocal microscopy. After incubation with cancer cells, the red fluorescence of IONAs largely overlapped with the green signal of lysosomes, demonstrating the efficient cancer cell uptake of IONAs (Figure 3b). It is worth noting that there is no obvious change in the numbers of lysosomes of the cells treated with/without IONAs. Moreover, when increasing the incubation duration from 0 to 2 h, both IONAs and Ins– IONAs showed corresponding and comparable increases in

their cellular uptake (Figures S27 and S28). However, with increasing the incubation time, only IONA-treated cells exhibited nonlinear amplification of the T1-weighted MR contrast compared with the Ins−IONA-treated cells (Figure 3c). These results indicate that the cross-linked IONAs are structurally robust before their cellular internalization. Once exposed to the acidic intracellular endo/lysosomal environment, the pH-sensitive hydrazone bonds are cleaved, resulting in the disassembly of the IONAs into dispersed ESIONs and therefore the enhancement of the T1MRI effect.[22]

To investigate the performance of IONAs in tumor MR diagnosis in vivo, IONAs were intravenously (i.v.) injected into tumor-bearing mice (Figure 4a). The in vivo stability of IONAs were examined by analyzing TEM and MRI data of the blood samples collected 15 min after the i.v. injection. As shown in Figure 4b,c and Figure S29, the structural morphology of both IONAs and Ins−IONAs in blood remained unchanged, and both nanoassemblies showed MR hypointensity. On the contrary, PIONAs suffered from serious dissociation in blood and exhibited a relatively higher T1MR signal, demonstrating the superior stability of such cross-linked nanoassemblies in blood flow.[33] At 1 h postinjection, the accumulated amount of nanomaterials in tumor regions was determined by inductively coupled plasma mass spectrometry (ICP-MS). The measured amounts of IONAs and Ins−IONAs were similar, but more than that of PIONAs (Figure S30), indicating that the IONAs can relatively suppress the false MR information in normal tissues by the enhanced localization to tumor regions. T1-weighted MR imaging results clearly indicated that IONAs could amplify the MR signal intensity as the postinjection time increased from 0 to 60 min. However, both Ins−IONAs and PIONAs showed significantly lower MR signals (Figure 4d and Figure S31). It is assumed that the improved tumor T1MR diagnosis by IONAs could be attributed to their pH-triggered disassembly with large q^{SS}. On the other hand, the inferior tumor MR imaging effect by PIONAs resulted from their small q^{SS} and lower tumor accumulation. The T1MR signal of Ins−IONAs was also low due to the T1MR-quenched state of the cross-linked ESIONs. In addition, T2-weighted MR imaging directly confirmed the dynamic reversibility of IONAs in vivo. In sharp contrast to the images obtained with the administration of either Ins−IONAs or PIONAs, the MR signal intensity of the surrounding normal tissues of tumor after the administration of IONAs was found to decrease in the first 30 min, followed by an enhancement from 30 to 60 min and a decrease again after 60 min, indicating the unique pH-dependent dynamic reversibility of IONAs between neutral normal tissues and acidic tumor regions (Figures S32 and S33).

The potential toxicology of IONAs in the mice was further explored. Pharmacokinetic studies revealed that IONAs have a blood circulation half-life time of ∼2.2 h, slightly longer than that of PIONAs (∼1.7 h) (Figure S34). Histopathological examinations showed no pathological change in heart, spleen, lungs, kidneys, and liver (Figures S35 and S36). Liver function evaluation (by measuring the serum levels of ALT, AST, TP, ALB, A/G, GLOB, and ALP) and kidney function evaluation (by measuring the serum levels of BUN and CREA) at 24 h and 15 days after IONA administration (Figures S37 and S38) further confirmed that IONAs caused no obvious hepatotoxicity or renal toxicity. All these in vivo results demonstrate that the highly biocompatible IONAs can serve as a qualified tumor pH-sensitive T1MR contrast agent.

In summary, a novel type of cross-linked iron oxide nanoparticle assemblies, IONAs, was designed and synthesized for the tumor pH-sensitive T1MR imaging. The cross-linked IONAs were highly stable at neutral pH even in extremely diluted conditions, which is advantageous over conventional polymer-assisted nanoparticle assemblies that generally lose their integration after dilution. Once exposed to the acidic environment, IONAs can readily disassemble into dispersed ESIONs, resulting in the enhancement of $r1$ relaxivity for the nonlinear amplification of T1MR signals for tumor detection. To our best knowledge, this is the first demonstration of the iron oxide nanoparticle-based MR contrast agent that can amplify the $r1$ relaxivity in acidic tumor microenvironment. We anticipate that the use of small-molecular linker ligands for cross-linking iron oxide nanoparticles into assemblies constitutes a major advancement in stimuli-responsive MR contrast agents and will be beneficial for medical imaging and drug delivery applications.

■ ASSOCIATED CONTENT

ⓢ Supporting Information

The Supporting Information is available free of charge on the ACS Publications website at DOI: 10.1021/acs.nanolett.8b04411.

> Materials and methods, ¹H NMR spectrum, XRD patterns, FT-IR spectra, additional TEM images, stability evaluation data, additional kinetic study, characterization of pH-sensitive structural reversibility, cell viability test results, biodistribution data, and biosafety evaluation data (PDF)

■ AUTHOR INFORMATION

Corresponding Author
*Tel.: +86-571-88208623. E-mail: lingds@zju.edu.cn.
ORCID ⓘ
Xiaolian Sun: 0000-0001-9549-4741
Taeghwan Hyeon: 0000-0001-5959-6257
Daishun Ling: 0000-0002-9977-0237
Author Contributions
○F.L., Z.L., and J.L. contributed equally to this work.
Notes
The authors declare no competing financial interest.

■ ACKNOWLEDGMENTS

■ REFERENCES

(1) Smith, B. R.; Gambhir, S. S. *Chem. Rev.* **2017**, *117*, 901−986.

(2) Glasser, M. F.; Coalson, T. S.; Robinson, E. C.; Hacker, C. D.; Harwell, J.; Yacoub, E.; Ugurbil, K.; Andersson, J.; Beckmann, C. F.; Jenkinson, M.; Smith, S. M.; Van Essen, D. C. *Nature* **2016**, *536*, 171−178.

(3) Chen, H.; Zhang, W.; Zhu, G.; Xie, J.; Chen, X. *Nat. Rev. Mater.* **2017**, *2*, 17024.

(4) Tucek, J.; Sofer, Z.; Bousa, D.; Pumera, M.; Hola, K.; Mala, A.; Polakova, K.; Havrdova, M.; Cepe, K.; Tomanec, O.; Zboril, R. *Nat. Commun.* **2016**, *7*, 12879.

(5) Ling, D.; Lee, N.; Hyeon, T. *Acc. Chem. Res.* **2015**, *48*, 1276−1285.

(6) Park, S.; Aalipour, A.; Vermesh, O.; Yu, J. H.; Gambhir, S. S. *Nat. Rev. Mater.* **2017**, *2*, 17014.

(7) Ni, D.; Bu, W.; Ehlerding, E. B.; Cai, W.; Shi, J. *Chem. Soc. Rev.* **2017**, *46*, 7438−7468.

(8) Perez-Balderas, F.; van Kasteren, S. I.; Aljabali, A. A. A.; Wals, K.; Serres, S.; Jefferson, A.; Soto, M. S.; Khrapitchev, A. A.; Larkin, J. R.; Bristow, C.; Lee, S. S.; Bort, G.; Simone, F. D.; Campbell, S. J.; Choudhury, R. P.; Anthony, D. C.; Sibson, N. R.; Davis, B. G. *Nat. Commun.* **2017**, *8*, 14254.

(9) Pöselt, E.; Kloust, H.; Tromsdorf, U.; Janschel, M.; Hahn, C.; Mablo, C.; Weller, H. *ACS Nano* **2012**, *6*, 1619−1624.

(10) Zhou, Z.; Tian, R.; Wang, Z.; Yang, Z.; Liu, Y.; Liu, G.; Wang, R.; Gao, J.; Song, J.; Nie, L.; Chen, X. *Nat. Commun.* **2017**, *8*, 15468.

(11) Wang, L.; Huang, J.; Chen, H.; Wu, H.; Xu, Y.; Li, Y.; Yi, H.; Wang, Y. A.; Yang, L.; Mao, H. *ACS Nano* **2017**, *11*, 4582−4592.

(12) Gallo, J.; Kamaly, N.; Lavdas, I.; Stevens, E.; Nguyen, Q.; Wylezinskaarridge, M.; Aboagye, E. O.; Long, N. J. *Angew. Chem., Int. Ed.* **2014**, *53*, 9550−9554.

(13) Osborne, E. A.; Jarrett, B. R.; Tu, C.; Louie, A. Y. *J. Am. Chem. Soc.* **2010**, *132*, 5934−5935.

(14) Yuan, Y.; Ding, Z.; Qian, J.; Zhang, J.; Xu, J.; Dong, X.; Han, T.; Ge, S.; Luo, Y.; Wang, Y.; Zhong, K.; Liang, G. *Nano Lett.* **2016**, *16*, 2686−2691.

(15) Zhou, H.; Tang, J.; Li, J.; Li, W.; Liu, Y.; Chen, C. *Nanoscale* **2017**, *9*, 3040−3050.

(16) Kim, B. H.; Lee, N.; Kim, H.; An, K.; Yong, I. P.; Choi, Y.; Shin, K.; Lee, Y.; Kwon, S. G.; Na, H. B.; Park, J. G.; Ahn, T.-Y.; Kim, Y.-W.; Moon, W. K.; Choi, S. H.; Hyeon, T. *J. Am. Chem. Soc.* **2011**, *133*, 12624−12631.

(17) Lu, Y.; Xu, Y.; Zhang, G.; Ling, D.; Wang, M.; Zhou, Y.; Wu, Y.; Wu, T.; Hackett, M. J.; Kim, B. H.; Chang, H.; Kim, J.; Hu, X.; Dong, L.; Lee, N.; Li, F.; He, J.; Zhang, L.; Wen, H.; Yang, B.; Choi, S. H.; Hyeon, T.; Zou, D. *Nat. Biomed. Eng.* **2017**, *1*, 637−643.

(18) Shen, Z.; Chen, T.; Ma, X.; Ren, W.; Zhou, Z.; Zhu, G.; Zhang, A.; Liu, Y.; Sone, J.; Li, Z.; Ruan, H.; Fan, W.; Lin, L.; Munasighe, J.; Chen, X.; Wu, A. *ACS Nano* **2017**, *11*, 10992−11004.

(19) Mesquita, S. D.; Louveau, A.; Vaccari, A.; Smirnov, I.; Cornelison, R. C.; Kingsmore, K. M.; Contarino, C.; Gumuscu, S.; Farber, E.; Raper, D.; Viar, K. E.; Powell, R. D.; Baker, W.; Dabhi, N.; Bai, R.; Cao, R.; Hu, S.; Rich, S. S.; Munson, J. M.; Lopes, M. B.; Overall, C. C.; Action, S. T.; Kipnis, J. *Nature* **2018**, *560*, 185−191.

(20) Viger, M. L.; Sankaranarayanan, J.; Lux, C. G.; Chan, M.; Almutairi, A. *J. Am. Chem. Soc.* **2013**, *135*, 7847−7850.

(21) Liu, J.; Bu, J.; Bu, W.; Zhang, S.; Pan, L.; Fan, W.; Chen, F.; Zhou, L.; Peng, W.; Zhao, K.; Du, J.; Shi, J. *Angew. Chem., Int. Ed.* **2014**, *53*, 4551−4555.

(22) Santra, S.; Jativa, S. D.; Kaittanis, C.; Normand, G.; Grimm, N.; Perez, J. M. *ACS Nano* **2012**, *6*, 7281−7294.

(23) Zhao, J.; Zhou, Z.; Jin, J.; Yuan, L.; He, H.; Jiang, F.; Yang, X.; Dai, J.; Liu, Y. *Chemosphere* **2014**, *100*, 194−199.

(24) Ling, D.; Park, W.; Park, S.; Lu, Y.; Kim, K. S.; Hackett, M. J.; Kim, B. H.; Yim, H.; Jeon, Y. S.; Na, K.; Hyeon, T. *J. Am. Chem. Soc.* **2014**, *136*, 5647−5655.

(25) Lu, J.; Sun, J.; Li, F.; Wang, J.; Liu, J.; Kim, D.; Fan, C.; Hyeon, T.; Ling, D. *J. Am. Chem. Soc.* **2018**, *140*, 10071−10074.

(26) Wu, L.; Mendoza-Garcia, A.; Li, Q.; Sun, S. *Chem. Rev.* **2016**, *116*, 10473−10512.

(27) Bao, Y.; Sherwood, J. A.; Sun, Z. *J. Mater. Chem. C* **2018**, *6*, 1280−1290.

(28) Fang, J.; Chandrasekharan, P.; Liu, X.; Yang, Y.; Lv, Y.; Yang, C.; Ding, J. *Biomaterials* **2014**, *35*, 1636−1642.

(29) Zhang, W.; Liu, L.; Chen, H.; Hu, K.; Delahunty, I.; Gao, S.; Xie, J. *Theranostics* **2018**, *8*, 2521−2548.

(30) Chen, C.; Ma, D.; Meany, B.; Isaacs, L.; Wang, Y. *J. Am. Chem. Soc.* **2012**, *134*, 7254−7257.

(31) Yang, C.; Tan, J. P. K.; Cheng, W.; Attia, A. B. E.; Ting, C. T. Y.; Nelson, A.; Hedrick, J. L.; Yang, Y. *Nano Today* **2010**, *5*, 515−523.

(32) Lv, S.; Wu, Y.; Cai, K.; He, H.; Li, Y.; Lan, M.; gChen, X.; Chen, J.; Yin, L. *J. Am. Chem. Soc.* **2018**, *140*, 1235−1238.

(33) Wang, Y.; Zhou, K.; Huang, G.; Hensley, C.; Huang, X.; Ma, X.; Zhao, T.; Sumer, B. D.; DeBerardinis, R. J.; Gao, J. *Nat. Mater.* **2014**, *13*, 204.

(34) Lattuada, M.; Hatton, T. A. *Langmuir* **2007**, *23*, 2158−2168.

(35) Bae, Y.; Fukushima, S.; Harada, A.; Kataoka, K. *Angew. Chem., Int. Ed.* **2003**, *42*, 4640−4643.

(36) Li, H.; Zhang, H.; Lammer, A. D.; Wang, M.; Li, X.; Lynch, V. M.; Sessler, J. L. *Nat. Chem.* **2015**, *7*, 1003−1008.

(37) Otter, C. A.; Patty, P. J.; Williams, M. A. K.; Waterland, M. R.; Telfer, S. G. *Nanoscale* **2011**, *3*, 941−944.

(38) Xu, C.; Yuan, X.; Kohler, N.; Kim, J.; Chung, M. A.; Sun, S. *J. Am. Chem. Soc.* **2009**, *131*, 15346−15351.

(39) Boros, E.; Gale, E. M.; Caravan, P. *Dalton Trans.* **2015**, *44*, 4804−4818.

(40) Zheng, X.; Zhao, K.; Tang, J.; Wang, X.; Li, L.; Chen, N.; Wang, Y.; Shi, S.; Zhang, X.; Malaisamy, S.; Sun, L.; Wang, X.; Chen, C.; Yan, C. *ACS Nano* **2017**, *11*, 3642−3650.

(41) Caravan, P. *Chem. Soc. Rev.* **2006**, *35*, 512−523.

(42) Shin, T.; Choi, Y.; Kim, S.; Cheon, J. *Chem. Soc. Rev.* **2015**, *44*, 4501−4516.

(43) Liu, Y.; Yang, Z.; Huang, X.; Yu, G.; Wang, S.; Zhou, Z.; Shen, Z.; Fan, W.; Liu, Y.; Davisson, M.; Kailish, H.; Niu, G.; Nie, Z.; Chen, X. *ACS Nano* **2018**, *12*, 8129−8137.

(44) Lee, Y.; Chen, D.; Dodd, S.; Bouraoud, N.; Koretsky, A.; Krishnan, K. *Biomaterials* **2012**, *33*, 3560−3567.

(45) Bai, C.; Jia, Z.; Song, L.; Zhang, W.; Chen, Y.; Zang, F.; Ma, M.; Gu, N.; Zhang, Y. *Adv. Funct. Mater.* **2018**, *28*, 1802281.

(46) Xie, H.; Zhu, Y.; Jiang, W.; Zhou, Q.; Yang, H.; Gu, N.; Zhang, Y.; Xu, H.; Xu, H.; Yang, X. *Biomaterials* **2011**, *32*, 495−502.

(47) Van Der Woude, I.; Wagenaar, A.; Meekel, A. A. P.; Ter Beest, M. B. A.; Ruiters, M. H. J.; Engberts, J. B. F. N.; Hoekstra, D. *Proc. Natl. Acad. Sci. U. S. A.* **1997**, *94*, 1160−1165.

(48) Lv, H.; Zhang, S.; Wang, B.; Cui, S.; Yan, J. *J. Controlled Release* **2006**, *114*, 100−109.

(49) Chen, H.; Li, P.; Yin, Y.; Cai, X.; Huang, Z.; Chen, J.; Dong, L.; Zhang, J. *Biomaterials* **2010**, *31*, 8172−8180.

(50) Roosjen, A.; Smisterova, J.; Driessen, C.; Anders, J. T.; Wagenaar, A.; Hoekstra, D.; Hulst, R.; Engberts, J. B. F. N. *Eur. J. Org. Chem.* **2002**, *2002* (7), 1271−1277.